Rheokinematics for Product Development – Formulation Screening in Rotational Rheometers

M.S.C.A. Brito[1], J. Matos[1], Marina V.L. Torres[1], C.P. Fonte[2], M.M. Dias[1], J.C.B. Lopes[1], R.J. Santos[1]*

[1] Laboratory of Separation and Reaction Engineering – Laboratory of Catalysis and Materials (LSRE-LCM), Universidade do Porto, Faculdade de Engenharia, Rua Dr Roberto Frias, 4200-465 Porto, Portugal

[2] Department of Chemical Engineering & Analytical Science, The University of Manchester, Oxford Road, Manchester, UK

[*]Email: rsantos@fe.up.pt

Abstract

Product formulations for industrial processes are typically developed at lab-scale. However, the mixing conditions are not easily mimicked in the lab. A rotational device is proposed in this work as a fast lab-scale formulation development, which enables mimicking the mixing conditions in the industrial process. The geometrical configurations of the rotational device are from rheometry devices (plate-plate and cone-plate). The main advantages of this method are the small amounts of raw materials, and shorter testing times. This methodology is applied to an industrial case study, the Reaction Injection Moulding (RIM) process. The mixing length scales evolution in the rotational rheometer were matched to those in RIM machines. The main novelty of this work is the introduction of a protocol that bridges the processing conditions at lab using small amounts of raw materials to high throughput continuous flow reactors.

Keywords: Product Development, Mixing, Rheometric Flow, Computational Fluid Dynamics, Reactive Polymerisation

1. Introduction

The development of new formulations that involve chemical reactions, such as, polymeric reactions, is a complex process that results in a significant number of experiments. The challenge of product development is related to a wide range of combinations between compositions and processing conditions, such as temperature, flow rates and mixing conditions. New techniques in formulation processes have been developed in order to reduce its complexity; for instance, the combinatorial library strategy where multiple collections of synthesised compounds are easily tested in a single process. For the development of new polymers, ceramics and metals, different methodologies have been implemented as high throughput techniques [1-5].

The automation of these processes has enabled the fast introduction of new materials and formulated products reducing the time to market by months and the costs of the inherent formulation processes. One of the advantages of robotic testing and analytics is the generation of robust and reproducible data many times faster than the traditional methods. In R&D centres, such as the Material Innovation Factory (MIF) at the University of Liverpool, robotics and high-performance computing have been used to accelerate the materials discovery and product development. The automated formulation robot (GEOFF), Formax, and high throughput rheometers are some of the automated technologies installed at MIF that enable the fast design of formulations [6, 7].

The implementation of high throughput material development methodologies is a current need in many industries. A procedure to design formulations at lab scale is presented in this paper to reduce the complexity of the product development. The objective is the development of a fast formulation process at the lab-scale with the advantage of requiring a small volume of reactants, which reduces waste and considerably speeds-up the process. This lab-scale method for product development must ensure the complex interactions between chemical

reaction and mixing of the reactants that occur at industrial scale. For that, characterisation of the mixing length scales and times in the lab-scale unit enables that this mixing scales evolution mimics the one at the industrial process scale.

One of the most challenging product development cases, as far as scale-up is regarded, is the formulation of reactive polymers for Reaction Injection Moulding (RIM). RIM is a common process for the production of PU and polyureas [8-11], where two highly viscous liquid monomers, isocyanate and polyol, are contacted as two high speed jets with a velocity range of $10-150\,ms^{-1}$ that are injected through two opposed injectors with $1-3\,mm$ of diameter. The two impinged liquid streams are mixed for $10-150\,ms$ in a cylindrical mixing chamber with diameter of $3-15\,mm$ and length around 5 times the diameter. At the outlet of the mixing chamber, the mixture is discharged at typical throughputs ranging from 10 $-100\,kg\,min^{-1}$ into a mould, where most of the polymerisation occurs, and a plastic part is formed [12]. The high volume production rates associated to this process, even for milli-sized RIM mixing chambers, imply quite expensive and lengthy procedures for formulation development [13-15].

The formulations for industrial RIM machines are usually designed at lab-scale and then tested in a pilot plant. The development of formulations at lab-scale usually occurs under mixing conditions, which do not correspond to the actual industrial or pilot-scale operational conditions. This makes, in most of the cases, the formulation recipe to fail in the production stage. The lab tests' lack of reproducibility in the pilot machines adds to this process cost and development time. The most time consuming step is associated to the filling of the storage tanks, which have a larger volume than 20 L, and to the raw materials and machine thermostabilisation prior to the mold injection. In addition, the efficient cleaning of the RIM machines when changing formulations during product development is an important step to avoids contaminations but it takes a long time. When the operating parameters in RIM

machines are not optimised, one of the most common problems at product development stages is the clogging of the mixing head caused by the polymerisation of the reactive mixture in the RIM mixing chamber nozzles. All above facts stress the need to set a methodology that enables the full control of mixing conditions at lab-scale for fast cost-effective product development processes .

In this work, shear rotational devices are addressed as lab units for fast product and formulation development. These devices are characterised by a laminar flow with a well-defined direction of shearing. The mixing in laminar flows, between two parallel plates, was described by Mohr et al. [16] using a dye dispersed into a fluid. Both fluids had the same viscosity and density and the diffusion between them was neglected. It was observed that the dye is stretched by the movement of the top wall. The result is the increase of the interface that separates the fluids creating thin lamellae of both fluids [17]. This visualisation of the mixing dynamics enables the full description of mixing from the deformation of the interfacial area [18] and the evolution of the striation thickness, that is, the typical scale of mixing of two segregated fluids [19, 20].

The pure shear flows generated in rheometric rotational devices have similar features to the ones addressed by Mohr et al. [16]. Rheometers measure the rheological properties of liquid samples, i.e., the dynamic viscosity, under controlled temperature and shearing/stress for a given period. The formulation development in rheometric devices is particularly interesting in the development of new products, because it provides a framework of fully controlled operational conditions while providing data relevant for the manufacturing industry, such as the gel time and the viscosity rise in the reactive system. This method can be easily adapted at polyurethane (PU) production sites to perform formulation studies to be used in RIM machines.

The main novelty of this paper is bridging the synthesis at small scale batch devices, used in laboratories for rheometry, to the operational conditions in continuous flow reactors with large throughputs. For this end, the evolution of the mixing dynamics and structures in plate-plate and cone-plate rheometer devices is described in this paper. The mixing length scales, i.e., the generation of the interfacial area and the striation thickness, are computed from CFD simulations and calculated from a Lagrangian approach. Different initial placement of fluids in the rheometer, the topology, will be studied to address its influence on the evolution of mixing length scales. Finally, the operational conditions in the rheometric device will be designed in order to generate the same mixing length scales as those in industrial RIM machines during the PU production. The main objective is the validation of the development of a formulation process for continuous flow reactors from small scale rheometric devices.

2. CFD model

2.1. 3D CFD Model

2.1.1. Physical Domain

The first flow geometry for laboratorial product development used in this work is a parallel plate-plate rotational rheometer. This geometry was introduced by Mooney [21] and consists in a disk rotating over a cylindrical cavity with slippery lateral walls. Figure 1a shows a sketch of two parallel plates used as the flow domain for the CFD simulations. In this work, the radius-to-height ratio is $R_P/h=5$, where $h=1\,mm$.

2.1.2. Boundary Conditions and Working Conditions

The top plate rotates at angular velocity ω and the bottom plate is stationary. In the 3D CFD simulation, the boundary conditions were set to the following particular values of the plates velocity: at the top plate, $\omega=0.01\,rad\,s^{-1}$, and at the bottom plate, $\omega=0\,rad\,s^{-1}$. At the top and bottom walls, no-split boundary conditions are assumed, i.e. the velocity components are set

to zero. The fluid enclosed between the two parallel plates has a density $\rho = 1260\, kg\, m^{-3}$ and a viscosity $\mu = 0.79\, Pa \cdot s$.

At this conditions, the Reynolds number, which is determined from $\Re = \rho \omega R_P h / \mu$, is $\Re = 8 \times 10^{-5}$, resulting in a creeping flow without secondary flow or flow separation.

2.1.3. Domain Discretisation and Governing Equations

The 3D domain was discretised with 6.6×10^6 elements uniformly sized hexahedral finite volumes with an edge length of $0.05\, mm$. The flow equations were simulated using Finite Volume software package ANSYS/Fluent to solve the continuity equation,

$$\nabla \cdot u = 0 \tag{1}$$

and the momentum equation,

$$\rho \left(\frac{\partial u}{\partial t} + u \cdot \nabla u \right) = -\nabla p + \mu \nabla^2 u \tag{2}$$

where u is the velocity vector, ρ and μ are density and viscosity, respectively, p is the pressure vector, and t is the flow time.

2.1.4. Steady Simulation

CFD simulations were first performed at steady-state, setting the dynamic term of Equation (2) equal to zero. SIMPLE scheme was used for the pressure-velocity coupling, and Second Order Upwind schemes were used for the spatial discretisation of pressure and advective terms of the momentum conservation equation. All flow variables were initialised with a value equal to zero, and the convergence criterion for the maximum residuals of continuity and momentum was 10^{-6}.

Figure 1b shows the velocity map obtained from the steady-state simulation. The velocity profile at the top plate is given by $\upsilon = \omega r$, and thus the velocity is $\upsilon = 0\, m\, s^{-1}$ at the top plate rotation axis ($r = 0$) and maximum at the plate radius, $r = R_P$, where $\upsilon_P = \omega R_P$ (see Figure 1b).

Therefore, the flow is described by a set of concentric circular streamlines, as shown Figure 1b.

Figure 1c shows the velocity vectors in the z-direction at $r \¿ R_P$ (using a cylindrical coordinate system) obtained from the steady-state CFD simulation. A linear velocity profile is generated between the two parallel plates. The rotation of the top plate induces the flow between the two plates causing the adjacent layers of fluid to slide over each other with different speeds due to the gradient of velocity in the z-direction.

Mooney [21] showed that, for a steady, laminar and isothermal flow and if $\upsilon_r = \upsilon_z = 0$ and considering no slip at the top and bottom plates, the velocity profile between the two parallel plates is given by

$$v_\theta(r,z) = \frac{r\omega z}{h} \tag{3}$$

where h is the space between plates and ω is the angular velocity of the top plate. Equation (3) shows that the velocity profile in the z-direction depends only on the radial position at the plate, r, and the height between plates, h [22].

Figure 2 shows the velocity profiles in z-direction at different distances from the rotation axis calculated from CFD simulations: $r = 0.1R_P$, $r = 0.5R_P$, $r = 0.9R_P$ and $r = R_P$ described by CFD simulation and the respective analytical expression (Equation (3)). This figure shows that Equation (3) is a good fit of the velocity profile obtained from 3D CFD simulations, validating the 3D CFD model. The CFD simulations were made to check the correct 3D description of this flow without imposing symmetry conditions and to generate the velocity field for the analysis of mixing in this device.

2.1.5. Dynamic Simulation

The flow field at steady-state conditions was used as the initial solution for the transient simulations of mixing. The flow of two similar fluids, i.e., fluids with the same properties,

between the two parallel rotational plates will enable the characterisation of the advective mixing mechanisms and the visualisation of the lamellar structure formed in well-defined shear conditions. Two different initial placements of fluids, that is, two different topologies, will be set to test the influence of topology on mixing.

The first initial condition consists of loading two similar fluids, black and white, side-by-side. This initial placement of the fluids is called Topology 1. Figure 3a shows the contour map of volume fraction of each fluid, black and white, at the initial instant, for Topology 1. The two fluids have the same physical properties: $\rho = 1260\, kg\, m^{-3}$ and $\mu = 0.79\, Pa \cdot s$.

A Eulerian-Eulerian approach is used with the Volume-of-Fluid (VOF) model to simulate the dynamics of mixing of two fluids in the flow. This model tracks the interface between two immiscible phases with equal physical properties. The surface tension and the diffusional mass transfer are neglected. For VOF simulation, a value of zero for the diffusion coefficient between the two phases is a good assumption for modelling of the mixing length scales.

In transient simulations, SIMPLE scheme was used for pressure-velocity coupling, PRESTO! and First Order Upwind were used for pressure and momentum. First Order Implicit scheme was used for the discretisation of the transient terms of momentum and continuity equations. Geometric Reconstruct scheme was set for the reconstruction of the interface position. The time step between iterations, Δt, was chosen according to the Courant number, $C_N = R_P t / x = 1$, where x is the edge length of an element of the discretisation grid.

Figure 3 shows the volume fraction contours maps for the mixing of two similar fluids in a parallel plate rotational device, initially placed according to Topology 1. Figure 3a corresponds to the initial time ($N = 0$), Figure 3b, Figure 3c and Figure 3d show the position of each phase after half-turn of the top plate ($N = 0.5$), one turn ($N = 1$) and two turns ($N = 2$), respectively. Figure 3 shows that the interfacial area between fluids is stretched out by the shear rate generated between the two parallel plates.

After one rotation of the top plate ($N=1$), the gap between plates is divided in two lamellae, one black strip and one white strip (Figure 3c) and after two turns (Figure 3d), the formation of a structure with four lamellae in the *z*-direction is observed. The formation of this lamellar structure is a result of the stretching of the interface between the representative fluids and respective deformation of each phase.

Another initial placement of the fluids is addressed in this work, Topology 2, that consists of the placement of two phases over each other, parallel to the rotating top plate. Figure 4 shows the contour map of the volume fraction of two fluids initially placed according to Topology 2 obtained from the dynamic CFD simulation. Figure 4a corresponds to the initial time, $N=0$, and Figure 4b to $N=1$. These results show that, for Topology 2, the interface between the two phases is not stretched and the lamellar structure does not change. At this working condition, the interfacial area between fluids is parallel to the velocity field, and so, the shear rate promotes the rotation of interface, remaining it invariant.

These results are the definitive proof that topology has an impact on mixing in laminar flows. The most efficient mixing of fluids achieved in the plate-plate rheometer corresponds to Topology 1. This means that when the interfacial area is initially placed perpendicularly to the velocity field, the interfacial area is increased by shearing. On the other hand, when the interfacial area has the same direction as the velocity field, the mixing length scales remain invariant.

The full characterisation of mixing in a plate-plate rheometer comprises the calculation of the mixing length scales, such as the growth of the interfacial area and the striation thickness decay. Matos et al. [23] proposed the Lagrangian Mixing Simulations (LMS) to quantity the mixing scales in laminar flows. This model uses particles to track the interface between two fluids to determine the interfacial area between fluids and the computation of segregation scales. LMS uses a Eulerian velocity field from a 2D CFD simulation of the flow. Thus, the

application of LMS over a plate-plate rheometer requires the modelling of 2D CFD simulations and the respective physical validation of the 2D results.

2.2. 2D CFD Model

2.2.1. Physical Domain and Discretisation

A 2D geometry physical representation of the flow in a plate-plate rheometer was set corresponding to the projection of the outer cylinder wall between the two parallel rotating plates. This domain consists of a rectangular geometry, where the top wall is moving, and the bottom wall is stationary. A relevant feature in plate-plate geometry is that the strain rate is not homogeneous along the radius. Mooney [21] demonstrated that the strain rate is $\dot{\gamma} = dv/dz = \omega r/h$ according to Equation (3). This dependence of the strain rate on the radius shows that the conditions of the projection of the outer circle are only valid for $r = R_p$. Thus, the evolution of mixing scale from this simulation is not valid for other circles, i.e. for any value of *r*.

Figure 5 shows the sketch of the domain simulated in 2D CFD simulation and the respective coordinate system. The geometrical parameters in Figure 5 do not correspond to 3D CFD simulations, i.e. the length of top wall does not correspond to the perimeter of the outer circle, $2\pi R_p$. The 2D geometry consists of two parallel walls with 10 mm length and spaced by 2 mm. Nevertheless, these dimensions are in the range of the typical geometrical conditions in rheometers.

The simulated domain was discretised with 10^5 rectangular elements. Grid was compressed in the y -direction, and so smallest grid elements with respect to height were generated around the walls. This refinement avoids numerical problems during the tracking of the interface between fluids, namely the slippage of the location of the interface between fluids. When the interface between the two fluid is inclined towards the horizontal direction by the flow action,

the layer of fluid next to the walls becomes very thin. If the mesh is not refined enough, the thinnest parts of the layer are erased and the contact points between the fluids at the walls, which are fixed, seem to slip. Care was taken to verify if the grid was enough for the description of mixing next to the walls.

2.2.2. Boundary Conditions and Working Conditions

The boundary conditions imposed on the simulation are the velocities of both walls: $v = 0\, m\, s^{-1}$ for the bottom wall, and $v_P = 1.4 \times 10^{-3} m\, s^{-1}$ for the top wall, which corresponds to an angular speed of $\omega = 0.87 \text{ rad s}^{-1}$ in a plate-plate rheometer presented previously. Periodic flow conditions were set on the right and left walls to simulate continuous flow in the entire domain, corresponding to the circular pathlines of the 3D geometry. This condition guarantees to simulate a closed circle as the outer wall in the 3D geometry. The fluid enclosed between the two parallel walls has the same physical properties set in 3D model: a density $\rho = 1260\, kg\, m^{-3}$ and a viscosity $\mu = 0.79\, Pa \cdot s$.

2.2.3. Steady Simulation

CFD simulations were initially performed at steady-state, setting the term of Equation (2) equal to zero. In steady-state simulations, SIMPLE scheme was used for the pressure-velocity coupling. Second Order and Second Order Upwind schemes were used for numerical spatial discretisation of pressure and advective terms of momentum equation.

The physical validation of 2D CFD steady-state solution was made from the 2D velocity profile, $v = R_P \omega y / h$ (using the cartesian coordinates of Figure 5). Results show that the analytical solution fits the CFD results. This validates the 2D model as a simplification of the 3D flow with direct application to the simulation of mixing.

2.2.4. Dynamic Simulation

The steady-state flow field was used as the initial solution for the dynamic CFD simulations. The flow of two similar fluids in 2D plate-plate rheometer was computed using the VOF model in ANSYS Fluent. SIMPLE scheme was set for the pressure-velocity coupling, PRESTO! and Second Order Upwind were used for pressure and momentum. First Order Implicit scheme was set for the discretisation of the transient terms of momentum equation and continuity equation. The reconstruction of the interface position between the two phases was made from Geometric Reconstruct scheme.

Mixing dynamics were simulated from the 2D model and with the initial condition according to Topology 1, that is, the 2D domain was initially divided into two similar fluids, black and white, side-by-side. The two fluids have the same physical properties, $\rho = 1260\, kg\, m^{-3}$ and $\mu = 0.79\, Pa \cdot s$.

Figure 6 shows the contour maps of the volume fraction of each fluid obtained from 2D CFD simulation at $N = 0$, $N = 1$ and $N = 2$. The number of turns, N, corresponds to the period of time that a particle takes to resume to the initial position. From $N = 0$ to $N = 2$, the interface is stretched by the shear rate, decreasing the striation thickness of each phase. Figure 6 shows that two lamellae are formed in the y-direction for $N = 1$, and four lamellae are generated for $N = 2$.

Figure 3c and 6b show two lamellae, black and white strips, are formed at $N = 1$, both for 3D as 2D CFD simulations. Figure 3d and 6c correspond to $N = 2$, where a structure with four lamellae are formed. Again, this comparison shows the 2D CFD simulation makes an accurate description of mixing in the actual 3D device.

2.2.5. LMS model

The validated 2D flow field in a plate-plate rotational rheometer can be applied to the Lagrangian Mixing Simuations, LMS, using the Eulerian velocity field. LMS follows the

process of interfacial area generation between two fluids by tracking a set of passive particles positioned at the interface. LMS was algorithm was implemented in Matlab using the velocity field from 2D CFD simulation. In LMS the position vector of each particle is determined by,

$$X_{i,j+\Delta t} = X_{i,j} + u_{i,j}\Delta t \tag{4}$$

where Δt is the time step, $u_{i,j}$ is the velocity vector of a particle, i represents the index of the particle and j is the index of the time step. The LMS algorithm was adapted using the methodology disclosed in Matos et al. [23].

The initial condition for the LMS corresponds to the placement of 35 particles into the left phase (red particles) and 35 particles into the right phase (black particles). Figure 7 shows the position of each cluster of particles in the 2D domain. Figure 7a corresponds to $N = 0$, Figure 7b and Figure 7c show the position of each particle for $N = 1$ and $N = 2$, respectively. Figure 7 clearly shows that the line formed by the cluster of particles, which is initially positioned through the gap between the two parallel plates, is stretched over the motion of the top wall. The overlapping of the phases causes the reduction of the striation thinning rate of each phase.

LMS enables the determination of the interfacial area between the two fluids, which corresponds to the length of the line that is formed by the loaded particles,

$$A(t) = \sum_{i=1}^{np} \left| X_{i,j} - X_{i,j+1} \right| \tag{5}$$

where *np* is the total number of particles. In Figure 8, the dashed line describes the dimensionless interfacial area, $\alpha'(t) = A(t)/A_0$, as a function of the number of turns, N, calculated from LMS. The initial interfacial area corresponds to the gap between parallel

plates, $A_0 = h$. The interface increases with the number of turns, as expected from 3D and 2D CFD simulations. The growth of the interfacial area is, on average, linear with time for $N > 0.5$.

Figure 7 shows that the interfacial area growth creates thin layers delimited by the tracking line. The concept of distance between two segregated fluids was defined by Mohr et al. [16] as the striation thickness. The striation thickness generated between the two parallel plates can also be calculated from LMS. For that, a medium point between two successive particles into the same fluid (x_1, y_1) is considered. Then a tangent to the current particle and the respective slope, m_1, was calculated. The perpendicular line to the tangent curve is obtained from $m_2 = 1/m_1$. The perpendicular line will cross the other interface, and the interception point is determined (x_2, y_2). Then the distance between interfaces can be determined by,

$$l_i = \sqrt{(x_{i+1} - x_i)^2 + (y_{i+2} - y_i)^2} \quad (6)$$

If the perpendicular curve does not cross the other interface, l_i is not calculated by LMS. This procedure is repeated for all particles in the flow front that is being tracked. The striation thickness corresponds to the minimum length from the set of line segments crossing both interfaces perpendicularly: $s = min\,(l_i)$. The same procedure is used for the complete time of the dynamic simulation.

The dashed line for s/s_0 axis in Figure 8 shows the mean normalised evolution of striation thickness as a function of the number of turns, *N*, calculated from LMS. The initial striation thickness, s_0, corresponds to half of the perimeter of the top plate, according to Figure 5 and the striation thickness decreases along of the number of turns. The validation of $\alpha'(t)$ and

$s(t)/s_0$ determined by LMS comprises the description of both mixing metrics from an analytical expression.

3. Kinematics of Deformation

In pure shear flows, as those generated in a plate-plate rheometer, mixing is characterised by the deformation of fluids. The stretching properties of flow are studied in this work from a Lagrangian point of view, tracking a passive material element. Figure 9 shows the deformation of a material element placed in a pure shear flow. This element of fluid is initially a square wherein the edges are dy and s_0. For $t>0$, the particle is deformed continuously by the flow and the edge dy is stretched out, causing the deformation of this length, dl, as shown in Figure 9.

The interfacial area and the striation thickness are easily quantified by the stretching of a material element illustrated in Figure 9. The evolution of interfacial area is described by $dl(t)$, and the striation thickness is given by the normal length between sides, which is represented by ds in Figure 9. The interfacial area and the striation thickness are quantified for the two topologies addressed in this work: Topology 1 (Figure 3) and Topology 2 (Figure 4).

In Topology 1, the two fluids are initially side-by-side. It was considered that an element of fluid corresponds to a single-phase and thus $dy \quad \Delta y=h$. The differential can be extended throughout the entire height because the interface is always a straight line. For $N=0$, the initial interfacial area corresponds to the gap between the two parallel plates, $A_0=h$. The evolution of the interfacial area, $A(t)$, is calculated from $dl(t)$, which is obtained from the motion of the top wall,dx, and the height of the domain, dy, as shown in Figure 9. It results in

$$dl(t)=\sqrt{dx^2+dy^2} \tag{7}$$

where $dx\ \Delta x(y=h)=v_P t$ for $dy\ \Delta y=h$. Thus, the dimensionless interfacial area, $\alpha'(t)=\frac{A(t)}{h}$, may be calculated from Equation Error: Reference source not found), resulting

$$\alpha'(t)=\sqrt{1+\left(\frac{\omega r t}{h}\right)^2} \tag{8}$$

where $\omega r=v_P$. This equation can be rewritten as a function of the number of turns since $t=NT$, where T is the time required for one complete turn, $T=2\pi/\omega$. So, Equation Error: Reference source not found) becomes $\alpha'(t)=\sqrt{1+(2\pi Nr/h)^2}$.

Mooney [21] demonstrated that the shear rate for a plate-plate geometry is given by $\dot{\gamma}=\omega r/h$, thus Equation Error: Reference source not found) can be rewritten according to the general expression, $\alpha'(t)=\sqrt{1+(\dot{\gamma}t)^2}$.

The evolution of striation thickness (ds in Figure 9) can also be calculated from the tracking of a material element. For an incompressible fluid, the relation between the initial striation thickness, s_0, and the evolution of striation thickness is given by

$$dy\, s_0=dl\, s \tag{9}$$

where dy, s_0, dl and s are illustrated in Figure 9. It was also considered that each fluid element corresponds to a single-phase ($dx\ \Delta x(y=h)=v_P t$ and $dy\ \Delta y=h$), the combination of Equation Error: Reference source not found) and Equation Error: Reference source not found results in

$$s(t)=\frac{s_0}{\sqrt{1+\left(\frac{\omega r t}{h}\right)^2}} \tag{10}$$

Equation Error: Reference source not found describes the reduction of striation thickness in a plate-plate rheometer. At $t=0$, the striation thickness is $s=s_0$ and for $t>0$, the lamellae striation thickness decreases due to the shear rate generated between the two plates. The general expression of $s(t)$ as a function of $\dot{\gamma}$ is given by $s(t)=s_0/\sqrt{1+(\dot{\gamma}t)^2}$.

The validation of Equations Error: Reference source not found and Error: Reference source not found comprises the comparison with LMS. Figure 8 shows the dimensionless interfacial area as a function of the number of turns calculated from LMS (dashed line) and from Equation Error: Reference source not found) (solid line). This plot clearly shows that Equation Error: Reference source not found) fits the LMS data making it a good prediction for the description of the dimensionless interfacial area in a plate-plate geometry.

Figure 8 also shows the evolution of striation thickness as a function of the number of turns calculated from LMS (dashed line) and Equation Error: Reference source not found (solid line). Equation Error: Reference source not found gives a good prediction of the decrease of the striation thickness along with the number of turns. Figure 8 shows that the fluid element undergoes a linear stretching and the respective evolution of striation thickness is given by $s(t)$ s_0/t, which is a feature of non-chaotic flows [24]. These results support the argument that the flow is non-chaotic at this range of Reynolds number.

Figure 10 shows the 2D phase position at $N=0$, $N=1$ and $N=2$ using Topology 2. The interfacial area at $N=0$ corresponds to the perimeter of the plate, $A_0=2\pi R_P$, which is illustrated by a red line in Figure 10. At $N=1$ and $N=2$, the interfacial area is $A(N=1)=2\pi R_P$ and $A(N=2)=2\pi R_P$, as shown in Figure 10 by the green line. From this

analysis, the evolution of the dimensionless interfacial area is given by $\alpha'(t)=1$ and the striation thickness is also independent of the number of turns and corresponds to half of the gap between the two plates, $s(t)=h/2$.

Demonstration of expressions of mixing metrics shows that a greater interfacial area is obtained for Topology 1 and so, thinner striation thicknesses are generated. For Topology 2, the mixing length scales are kept constant with the number of turns. Therefore, topology plays an important role in the evolution of mixing scales in mixing devices. Table 1 summarises the analytical expressions that describe mixing length scales for Topologies 1 and 2.

The fluid dynamics and the evolution of the mixing length scales were also described for cone-plate rheometers. Figure 11 shows the sketch of a cone-plate geometry of rotational rheometers and a schematic representation of the gap between cone and plate. In this case, the velocity profile is given by,

$$\upsilon_\theta(r,z)=\frac{r\omega}{\beta}\arctan\frac{z}{r} \tag{11}$$

where β is the cone angle [22]. For this geometry, the shear rate is constant at every radial location in the cone-plate geometry, $\dot{\gamma}=\omega/\beta$ [22]. Since the flow between cone and plate has uniform shear conditions in the entire domain, it is possible to simulate the flow field in a 2D domain which corresponds to the projection of the outer circle of the geometry for $r=R_p$ and $z\in[0,h]$. Therefore, the 2D CFD simulation presented previously for the plate-plate configuration can also represent the flow field from a representative part of the cone-plate 3D flow and the mixing length scale can be obtained from that simulation. For a cone-plate geometry and for the initial conditions according to Topology 1, the analytical equations of the interfacial area and striation thickness can be described from the general expressions where $\dot{\gamma}=\omega/\beta$: $\alpha'(t)=\sqrt{1+(\omega t/\beta)^2}$ and $s(t)=s_0\left(1+(\omega t/\beta)^2\right)^{-1/2}$.

Table 1summarises the relationships of the dimensionless interfacial area and striation thickness evolution for plate-plate geometry with Topologies 1 and 2, and for cone-plate geometry with Topology 1. Topology 2 is not analysed for cone-plate because the two boundaries are not parallel and so the two liquids would have to be overlaid with an interface located at the bisection of angle β. This initial placement of the two fluids is not practical and would require the development of particular technology for liquids injection into the geometry.

Table 1 Mixing scales length obtained in Topology 1 and 2

		Interfacial Area	**Striation Thickness**
Topology 1, plate-plate	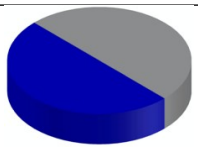	$\alpha'(t)=\sqrt{1+\left(\frac{\omega r t}{h}\right)^2}$	$s(t)=\frac{s_0}{\sqrt{1+\left(\frac{\omega r t}{h}\right)^2}}$
Topology 2, plate-plate	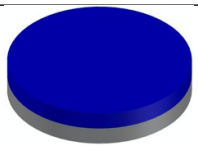	$\alpha'(t)=1$	$s(t)=\frac{h}{2}$
Topology 1, cone-plate	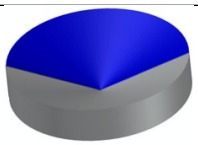	$\alpha'(t)=\sqrt{1+\left(\frac{\omega t}{\beta}\right)^2}$	$s(t)=\frac{s_0}{\sqrt{1+\left(\frac{\omega t}{\beta}\right)^2}}$

4. Product development for RIM

One of the objectives of this work is the implementation of a formulation process in plate-plate or cone-plate rheometers as a methodology for high throughput material development. This method is quite useful to determine the exact evolution of mixing scales in products made from chemical processes. In this work, the CIJs (Confined Impinging Jets) reactor used in RIM is used as a case study on the implementation of this methodology for product

development. The CIJ mixing chamber in RIM machines operates at production rates from 10 to 100 kg min^{-1}. Furthermore, the actual mixing conditions in the CIJs have an impact on the final RIM products, as it has been shown in previous works mainly for PU moulded parts [10, 25-28], and studied using test reactions for assessment of micromixing [29-31]. In general, product development for RIM is made with actual production conditions in pilot machines, and thus the formulations screening becomes a lengthy process. Typically, the operations involved in setting the new raw materials for a formulation testing, include thermostabilising, tank cleaning and filling, and this whole process may take longer than one hour. The development of a methodology for the pre-screening of RIM formulations in plate-plate or cone-plate devices enables accelerating product development with the advantage of decreasing quantities of testing raw materials from the scale of kilograms to grams.

In RIM machines, mixing is promoted by the contact of two jet streams injected in a confined mixing chamber at high velocities [8-11]. In the case of RIM for PU production, a stream would be an isocyanate and the other a polyol. Figure 12a is a sketch of a typical CIJ for RIM machines with a cylindrical mixing chamber and two opposed round injectors. The mixing chamber diameter is D ($3 \le D \le 10\,mm$), and the inlet chamber diameter is d ($1 \le d \le 3\,mm$). The top left sketch of Figure 12a corresponds to a cross-view in the normal direction of the injectors axis, and the bottom right sketch of Figure 12a is the front view.

Figures 12b, 12c and 12d show Planar Laser Induced Fluorescence (PLIF) images of concentration fields for different mixing conditions. The PLIF images are at the same conditions of Fonte et al. [32], $d = 1.5\,mm$, $D = 10\,mm$ and fluids were glycerol aqueous solutions with $\mu = 20\,mPa \cdot s$ and $\rho = 1180\,kg\,m^{-3}$. Figure 12b and 12c show the mixing of a dyed stream, white colour issuing from left-hand side, and a clear stream, dark colour issuing from right-hand side. A dashed line shows the axis of the injectors in the figure. Figure 12b shows a segregated flow regime, with clear and dyed stream flowing side by side, and Figure

12c is obtained at the onset of chaotic flow regime, and so this is the operating condition for the mixing of the two liquid streams in RIM. Detailed analysis of flow regimes in CIJs from PLIF and other visualisation techniques is well-established in the literature [33-35].

As shown in Figure 12b and 12c, the impingement of the two streams promotes the formation of a pancake at the point where liquids contact, as observed by Wood et al. [36]. Effective mixing occurs due to the stretching of the interface between the fluids, and thus the formation of a lamellar structure composed of the two phases (Figure 12c). For the exact screening of the 2D information, the evolution of the lamellar structure was assessed in each region of the mixing chamber working at chaotic flow regime. The three regions identified from PLIF images are: in the contact point between jets where a pancake is formed, in the mixing zone where a vortex street is formed and in a region downstream where a fully developed laminar flow is generated.

The segregated flow regime image (Figure 12b) is useful for the analysis of the initial contact of the two flow streams, because the interfaces are clear. When the two opposed jets impinge in CIJs they spread radially, forming a pancake like structure [36]. The flow spreading occurs nearly without deceleration of the injection velocity in the mixing chamber, υ_{inj}, following a pattern that is schematically depicted in Figure 12a from two views. The scale analysis starts at a radial distance of $d/2$ from the jets impingement point (Figure 12b). Considering that the jets inlet velocity is υ_{inj}, each inlet flow rate is $q_{inj}=\upsilon_{inj}\pi d^2/4$. The implementation of the mass conservation to the ring around the jet at $r=d/2$ results

$$q_{inj}=\upsilon_{inj}2\pi r(t)s \tag{12}$$

where $r(t)$ and s are the radial direction and the striation thickness, respectively, which are represented in Figure 12a. Considering that the striation thickness is s_0 at $r=d/2$, $s_0=d/4$

from Equation (12). This position is illustrated in Figure 12b. Assuming the velocity does not decrease in the pancake [37, 38], the striation thickness decreases with the radius as,

$$\frac{s(t)}{s_0}=\frac{d}{2r(t)} \tag{13}$$

Considering an element in the pancake interface, the dependence of the particle position with the time is $t=r(t)/\upsilon_{inj}$. This results in

$$\frac{s(t)}{s_0}=\frac{d}{2\upsilon_{inj}t} \tag{14}$$

At the end of the pancake spreading ($r(t)=D/2$), the striation is $s_1/s_0=d/D$ according to Equation Error: Reference source not found, where index 1 in s_1 stands for the striation thickness at the end of the pancake.

The segregated flow regime was used to illustrate the initial thinning of the raw materials, but the mixing efficiency in this regime is not sufficient for industrial fast polymerisation processes [11, 32, 36, 38]. For PU processing, the operation must occur at chaotic flow regime, where after the initial thinning of the raw materials, further mixing occurs by engulfment in vortices that are formed around the inlet jets [33, 34, 38, 39]. These vortices are clear from Figure 12c, and extend through a distance of approximately half a mixing chamber diameter, $D/2$. The shedding frequency of these vortices is given by the velocity oscillations frequency at the jets impingement point that is widely reported in the literature [35, 36, 38, 40, 41]. A typical value for this shedding frequency is $St\approx 0.06$, where St is the Strouhal number, $St=\phi d/\upsilon_{inj}$ [38, 42]. The vortex shedding frequency, ϕ, corresponds to an average period of shearing in this flow structures of $T=1/\phi$. These vortices radius is $D/4$ with average velocity in the periphery of υ_{inj}, and thus the shear rate in radial direction of

these vortices is $\dot{\gamma}=4\upsilon_{inj}/D$. Considering that the fluids strias are oriented in the angular direction in these vortices, as can be seen from Figure 12c, a pure shear flow could be used as a good approximation of the flow dynamics in CIJs. So, the striation thinning in this region is,

$$\frac{s(t)}{s_1}=\frac{1}{\sqrt{1+\dot{\gamma}^2t^2}}=\frac{1}{\sqrt{1+\left(\frac{4\upsilon_{inj}}{D}\right)^2t^2}} \tag{15}$$

The final striation thickness can be determined from the average shedding period of these vortices, $t=T=1/\phi$. The resulting striation thickness is,

$$\frac{s_2}{s_1}=\frac{1}{\sqrt{1+\frac{16d^2}{St^2D^2}}} \tag{16}$$

where the index 2 in s_2 is the striation thickness after the mixing region with vortex shedding.

After the engulfment region, the vortices are rapidly involved in the region defined by an approximate parabolic flow profile where the average shear rate is $\dot{\gamma}=2\upsilon_{mean}/D$ (Figure 12d). The mean velocity, υ_{mean}, is determined by the mass conservation between the inlet and the outlet and so $\upsilon_{mean}=2\upsilon_{inj}d^2/D^2$. Considering a pure shear flow in this region, the striation thickness rate is,

$$\frac{s(t)}{s_2}=\frac{1}{\sqrt{1+\frac{16v_{inj}^2d^4}{D^6}t^2}} \tag{17}$$

The striation thinning rate in CIJs can be matched to that of a plate-plate device from its angular velocity, as listed in Table 2. The striation thickness evolution and the respective plate angular velocity are plotted in Figure 13, where different values angular velocity correspond to markedly different regions in CIJs. The CIJ considered for the calculations has a length of $5D$, injectors diameter of $d=1.5mm$, a mixing chamber diameter of $D=10mm$, and inlet jets velocity of $v_{inj}=4ms^{-1}$. The corresponding plate-plate analysis was made for an $R_p=10cm$ and $h=d/4=0.345mm$.

The final striation in the plot of Figure 13 is $s=0.01s_0\approx 3.5\mu m$ in this case. Depending on the path of different fluid elements, the striation thickness varies. So, the sampling of annular sections of the final material properties at different mixing histories can be obtained from a single test.

The final striation in the plate-plate depends on the material being analysed. Data on small scale interfacial phenomena in PU synthesis shows that in the $10\mu m$ range there are other "mixing" mechanisms besides convection [43, 44]. So, for the PUs case, there is evidence that a final striation of $10\mu m$ is enough for material synthesis aiming fast product development.

An interesting fact from the analysis of Figure 12 is that in RIM machines, the topology also plays a major role in the evolution of mixing scales. Different topologies of the fluid interface are associated to different flow regimes. An analogy between the topology set in the plate-plate geometry and CIJs flow regimes can be done: Topology 1 corresponds to chaotic flow regimes, where there is the formation of vortices that reduce the mixing scales, while Topology 2 corresponds to the segregated flow regime where the interface between two phases is preserved without any change. Although the segregated flow regime has vortices engulfing fluid, these vortices are placed in opposed sides of the chamber failing in this way to engulf fluid from both jets.

Table 2 Mixing scales length evolution in CIJs and related evolution in plate-plate device

	CIJs	Period	Plate-Plate angular velocity
Pancake shearing	$\frac{s(t)}{s_0}=\frac{d}{2\upsilon_{inj}t}$	$\frac{d}{2\upsilon_{inj}}\le t<\frac{D}{2\upsilon_{inj}}$	$\omega(t)=\frac{h}{R_p t}\sqrt{\left(\frac{2\upsilon_{inj}t}{d}\right)^2-1}$
Engulfing vortices	$\frac{s(t)}{s_1}=\frac{1}{\sqrt{1+\left(\frac{4\upsilon_{inj}}{D}\right)^2 t^2}}$	$\frac{D}{2\upsilon_{inj}}\le t<\frac{d}{St\,\upsilon_{inj}}$	$\omega(t)=\frac{4\upsilon_{inj}h}{D\,R_p}$
CIJs runner	$\frac{s(t)}{s_2}=\frac{1}{\sqrt{1+\frac{16\upsilon_{inj}^2 d^4}{D^6}t^2}}$	$\frac{d}{St\,\upsilon_{inj}}\le t$	$\omega(t)=\frac{4d^2\upsilon_{inj}h}{D^3 R_p}$

Experimental studies on this new rheometric methodology for PU synthesis have been described by Torres [45]. The experiments were carried out with a cone-plate configuration with an angle of 0.017 rad and a diameter of 50 mm. The objective of the implementation of this new methodology was to analyse the lab product development method for the fast mixing and curing of two reactive monomers before it is implemented in an industrial RIM machine. A commercial Huntsman formulation of polyurethanes RenCast FC 52 Isocyanate / FC 52 Polyol was used, with curing times in the 15 min range. A holding cell with a separator was used to lay the fluids in the plate according to initial condition of Topology 1. The effect of the premixing shear rate on the gel time was obtained from the oscillatory test using the following conditions: duration of premixing ratio interval 100 s at constant rotational mode in a range of shear rates from 100 to 1000 s^{-1} (corresponding to cone angular velocities of $1.7\le\omega\le17\,rad/s$); after the pre-mixing stage, the storage modulus was dynamically measured with an oscillatory test with an angular frequency of 50 s^{-1} and a strain of 1%. Figure 14 shows the complex viscosity against the premixing shear rate as a changing parameter. For higher premixing shear rates, i.e. for more intense premixing conditions, the

build-up of storage modulus was faster. Although the kinetics of this PU formulation is considerably slower than industrial RIM formulations, that have curing times of around 2 min, the initial contacting history played a key role in the polymerisation reaction. This is clear evidence of the key role that mixing plays in the product development of complex reactive processes.

5. Conclusion

Rotational mixers based on rheometric devices were applied for high throughput material development for reactive processes. Two rheometric configurations were addressed in this work: plate-plate and cone-plate. Mixing for these devices was quantified, and design equations were introduced in terms of striation thinning and interfacial area generation. CFD simulations and LMS showed that a larger interfacial area is obtained for Topology 1, that is when the two fluids are initially placed side-by-side, resulting in thinner striation thicknesses. For Topology 2, where the fluids are initially placed one on top of the other, the mixing length scales remain unchanged with the number of turns of the top plate. These results prove that the topology plays an important role in the evolution of mixing scales in the mixing devices. The application of this product development procedure to an actual reactive polymerisation industrial process was made for a case study, the RIM process. This high throughput material development method enables to reduce quantities of raw materials in the product development from the kilograms range to grams and to shorten the testing cycles from hours to minutes. In addition to the full control of testing conditions in rotational devices, the mixing conditions are related to industrial processing, which enables direct process scale-up from this product development procedure.

Acknowledgements

This work was financially supported by: Base Funding - UIDB/EQU/50020/2020 of the Associate Laboratory LSRE-LCM - funded by national funds through FCT/MCTES (PIDDAC), by POCI-01-0145-FEDER-016851 and by POCI-01-0145-FEDER-030445 – funded by FEDER funds - Programa Operacional Competitividade e Internacionalização (POCI) – and by national funds through FCT - Fundação para a Ciência e a Tecnologia I.P; and by FCT scholarships PD/BD/135060/2017 and SFRH/BD/137094/2018.

Notation

$A(t)$ – interfacial area [m]

A_o – initial interfacial area [m]

C_N – Courant Number

d – diameter of injectors [m]

$dl(t)$ – interfacial area of an element of fluid [m]

dx – edge of an element of fluid [m]

dy – edge of an element of fluid [m]

D – diameter of the mixing chamber [m]

h - gap between two plates [m]

i – particle

j – time

l_i – distance between interfaces

m_1 – slope of the coordinates of two successive particles

m_2 – the inverse of m_1

N – number of turns

p – pressure [Pa]

q_{inj} – inlet flow rate [m^3/s]

r – radial coordinate [m]

R_P – radius of plate [m]

s – striation thickness [m]

s_0 – initial striation thickness [m]

s_1 – final striation thickness at the formation of pancake[m]

s_2 – final striation thickness formed from vortices [m]

St – Strouhal number

t – time [s]

T - period [s]

u – velocity vector field [m/s]

x – space coordinate [m]

X – position vector [m]

y – space coordinate [m]

z – cylindrical coordinate [m]

Greek letters

α' – dimensionless interfacial area

β – angle between cone and plate [rad]

$\dot{\gamma}$ – shear rate [s^{-1}]

Δt – time step [s]

Δx – edge of one element of the mesh [m]

θ – cylindrical coordinate [rad]

μ – viscosity [Pa·s]

ρ – density [kg/m^3]

υ – velocity [m/s]

υ_{inj} – inlet velocity [m/s]

υ_{mean} – mean velocity at the region of parabolic profile [m/s]

υ_P – velocity of the top plate [m/s]

υ_r – velocity in the radial coordinate [m/s]

υ_z – velocity in the z coordinate [m/s]

υ_θ – velocity in the θ coordinate [m/s]

ϕ – vortex shedding frequency [Hz]

ω – angular velocity [rad/s]

References

1. Akinc, A., et al., *Parallel Synthesis and Biophysical Characterisation of a Degradable Polymer Library for Gene Delivery.* Journal of the American Chemical Society, 2003. **125**(18): p. 5316-5323.
2. Zhang, H., et al., *Combinatorial and high-throughput approaches in polymer science.* Measurement Science and Technology, 2004. **16**(1): p. 203-211.
3. Wu, T., et al., *Formation and Properties of Anchored Polymers with a Gradual Variation of Grafting Densities on Flat Substrates.* Macromolecules, 2003. **36**(7): p. 2448-2453.
4. Zhao, J.-C., *Combinatorial aproaches as effective tools in the study of phase diagrams and composition-structure-property relationships.* Progress in Materials Science, 2006. **51**: p. 557–631.
5. Springer, H. and D. Raabe, *Rapid alloy prototyping: Compositional and thermo-mechanical high throughput bulk combinatorial design of structural materials based on the example of 30Mn–1.2C–xAl triplex steels.* Acta Materialia, 2012. **60**(12): p. 4950-4959.
6. Unilever, *Fast tracking discovery at the Materials Innovation Factory*, in *Unilever's News*. 2018.
7. Liverpool, U.o. *Materials Innovation Factory*. 2019 [cited 2019 April 2019]; https://www.liverpool.ac.uk/materials-innovation-factory/].
8. Malguarnera, S.C. and N.P. Suh, *Liquid injection molding I. An investigation of impingement mixing.* Polymer Engineering & Science, 1977. **17**(2): p. 111-115.
9. Ritcher, E.B. and C.W. Macosko, *Kinetics of Fast (RIM) Urethane Polymerisation.* Polymer Engineering and Science, 1978. **18**(13).
10. Lee, L.J., et al., *Impingement mixing in reaction injection molding.* Polymer Engineering & Science, 1980. **20**(13): p. 868-874.
11. Tucker, C.L. and N.P. Suh, *Mixing for reaction injection molding II. Impingement mixing of fiber suspensions.* Polymer Engineering & Science, 1980. **20**(13): p. 887-898.
12. Oertel, G., *Polyurethane Handbook*. 1985, Munich: Hanser.
13. Berins, M.L., *Plastics Engineering Handbook of the Society of the Plastics Industry*. 5th ed. ed. 1991: Kluwer Academic Publishers.
14. Macosko, C.W., *RIM, Fundamentals of Reaction Injection Molding*. 1989: Hanser Publishers.
15. Ranz, W.E., *Analysis of reaction processes in which microscopic heterogeneities appear: Scale-up and scale-down of polymerisation reactions*. Vol. 25. 1986.
16. Mohr, W.D., R.L. Saxton, and C.H. Jepson, *Mixing in Laminar-Flow Systems.* Industrial and Engineering Chemistry, 1957. **49**(11): p. 1855-1856.
17. Ottino, J.M., W.E. Ranz, and C.W. Macosko, *A lamellar model for analysis of liquid-liquid mixing.* Chemical Engineering Science, 1978. **34**: p. 877-890.

18. Spencer, R.S. and R.M. Wiley, *The mixing of very viscous liquids.* Journal of Colloid Science, 1951. **6**(2): p. 133-145.
19. Ranz, W.E., *Applications of a Stretch Model Diffusion, and Reaction in Laminar and Turbulent Flows.* AlChE Journal 1979. **25**.
20. Mohr, W.D., R.L. Saxton, and C.H. Jepson, *Theory of Mixing in the Single-Screw Extruder.* Industrial & Engineering Chemistry, 1957. **49**(11): p. 1857-1862.
21. Mooney, M., *A Shearing Disk Plastometer for Unvulcanized Rubber.* Industrial & Engineering Chemistry Analytical Edition, 1934. **6**(2): p. 147-151.
22. Macosko, C.W., *RHEOLOGY Principles, Measurements and Applications*. 1993, Minneapolis.
23. Matos, J., et al., *Lagrangian mixing simulation and quantification of scales.* Chemical Engineering Science, 2018. **192**: p. 199-210.
24. Ottino, J.M. and S. Wiggins, *Introduction: mixing in microfluidics.* Philosophical transactions of the royal society, 2004.
25. Gomes, N.M.O., et al., *Real time control of mixing in Reaction Injection Moulding.* Chemical Engineering Research and Design, 2016. **105**: p. 31-43.
26. Kolodziej, P., C.W. Macosko, and W.E. Ranz, *The influence of impingement mixing on striation thickness distribution and properties in fast polyurethane polymerisation.* Polymer Engineering & Science, 1982. **22**(6): p. 388-392.
27. Kolodziej, P., et al., *Impingement mixing and its effect on the microstructure of RIM polyurethanes.* Journal of Polymer Science Part B: Polymer Physics, 1986. **24**(10): p. 2359-2377.
28. Nguyen, L.T. and N.P. Suh, *Effect of High Reynolds Number on the Degree of Mixing in RIM Processing.* Polymer Process Engineering, 1985. **3(1&2)**: p. 37-56.
29. Brito, M.S.C.A., et al., *Fully resolved modelling and simulation of micromixing in confined impinging jets.* Chemical Engineering Science, 2020. **211**: p. 115299.
30. Kusch, H.A., J.M. Ottino, and D.M. Shannon, *Analysis of impingement mixing-reaction data: use of a lamellar model to generate fluid mixing information.* Industrial & Engineering Chemistry Research, 1989. **28**(3): p. 302-315.
31. Nunes, M.I., et al., *Micromixing assessment of confined impinging jet mixers used in RIM.* Chemical Engineering Science, 2012. **74**: p. 276-286.
32. Fonte, C.P., et al., *Flow imbalance and Reynolds number impact on mixing in Confined Impinging Jets.* Chemical Engineering Journal, 2015. **260**: p. 316-330.
33. Unger, D.R. and F.J. Muzzio, *Laser-induced fluorescence technique for the quantification of mixing in impinging jets.* AIChE Journal, 1999. **45**(12): p. 2477-2486.
34. Nakamura, S. and R. Brodkey, *Direct and Large Eddy Simulation of the Three-Dimensional Unsteady Flows in the Counter-Jet Mixing Vessel.* American Society of Mechanical Engineers, Fluids Engineering Division (Publication) FED, 2000. **251**: p. 947-954.

35. Shi, Z.-h., et al., *Experimental study of mixing enhancement of viscous liquids in confined impinging jets reactor at low jet Reynolds numbers.* Chemical Engineering Science, 2015. **138**: p. 216-226.
36. Wood, P., et al., *Experimental and computational studies of the fluid mechanics in an opposed jet mixing head.* Physics of Fluids A, 1991. **3**(5): p. 1362-1368.
37. Santos, R.J., et al., *Hydrodynamics of the mixing chamber in RIM: PIV flow-field characterisation.* AIChE Journal, 2008. **54**(5): p. 1153-1163.
38. Santos, R., J., et al., *Dynamic Behavior of the Flow Field in a RIM Machine Mixing Chamber.* AIChE Journal, 2009. **55**: p. 1338-1351.
39. Zhao, Y. and R.S. Brodkey, *Averaged and Time-resolved Full-field (three-dimensional), Measurements of Unsteady Opposed Jets.* The Canadian Journal of Chemical Engineering, 1998. **76**: p. 536-545.
40. Li, W.-F., et al., *Experimental investigation of flow regimes of axisymmetric and planar opposed jets.* AIChE Journal, 2011. **57**(6): p. 1434-1445.
41. Li, W.-F., et al., *Experimental study of oscillation behaviors in confined impinging jets reactor under excitation.* AIChE Journal, 2015. **61**(1): p. 333-341.
42. Gonçalves, N.D., et al., *On the 2D nature of flow dynamics in opposed jets mixers.* AIChE Journal, 2017. **63**(6): p. 2335-2347.
43. Machuga, S.C., et al., *Microdispersive interfacial mixing in fast polymerisations.* AIChE Journal, 1988. **34**(7): p. 1057-1064.
44. Wickert, P.D., W.E. Ranz, and C.W. Macosko, *Small scale mixing phenomena during reaction injection moulding.* Polymer, 1987. **28**(7): p. 1105-1110.
45. Torres, M.V.L., *An experimental procedure for Reaction Injection Moulding – RIM – material formulation design*, in *Chemical Engineerinh*. 2014, University of Porto: Portugal.

Figures

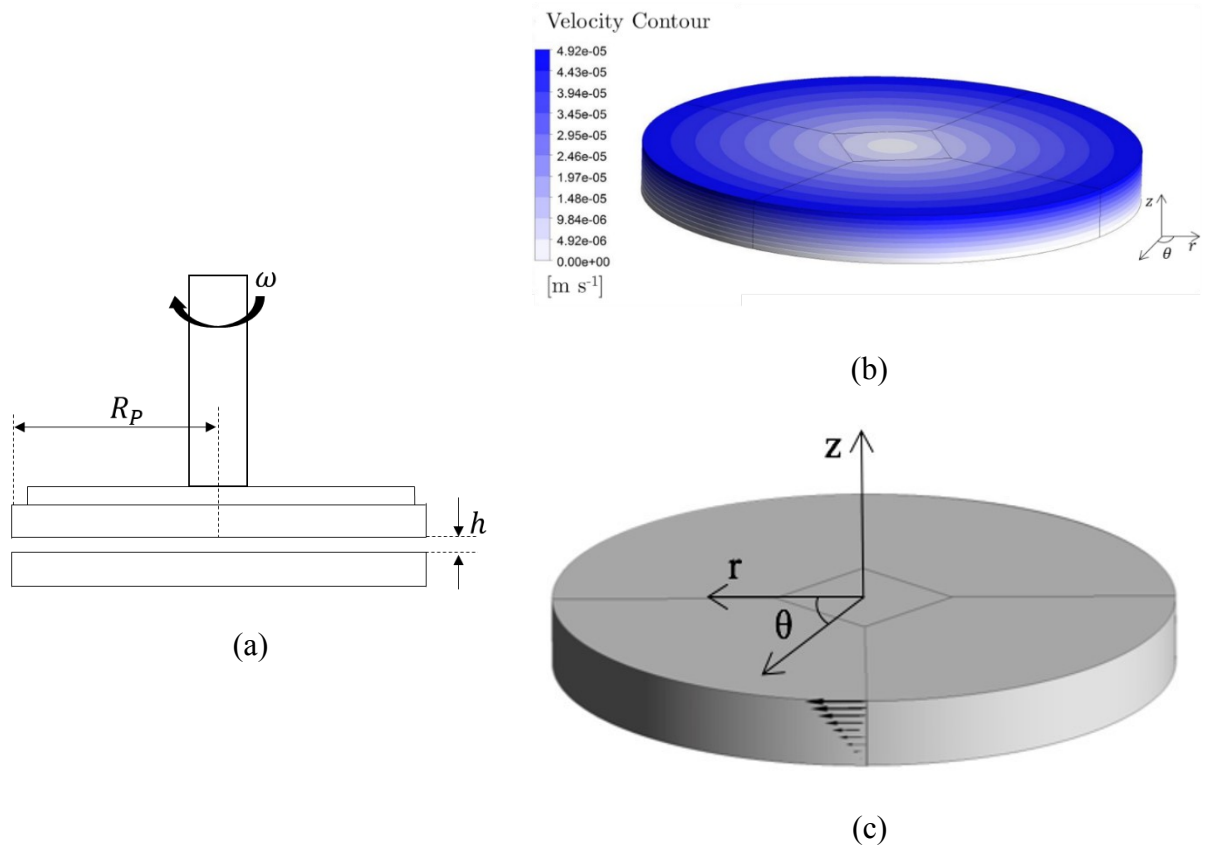

Figure 1 – (a) Sketch of a 3D parallel plates rheometer where R_P is the radius of the plate, h is the gap between the two parallel plates and ω is the angular speed of the top plate; (b) Velocity magnitude maps in parallel plates rheometer; (c) Velocity profile in the z-direction and cylindrical coordinates system.

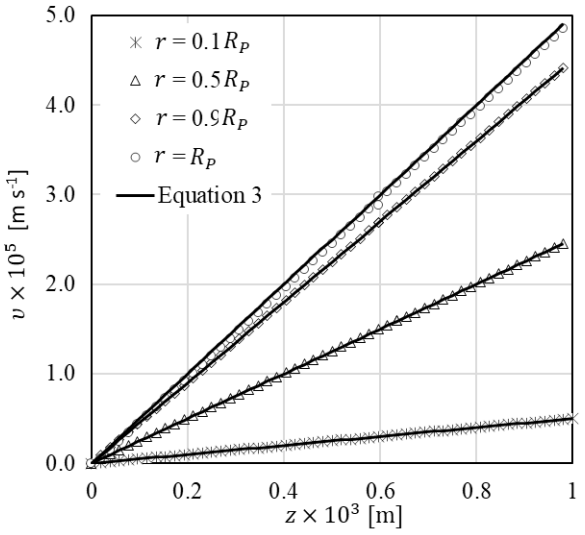

Figure 2 – Velocity profiles in the z-direction at different positions of the centre for plate/plate rheometer: symbols correspond to CFD simulation and lines corresponds to Equation (3).

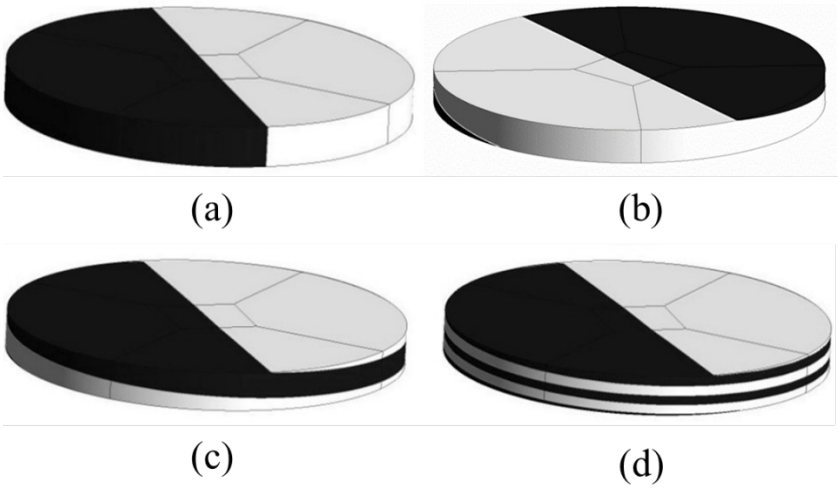

Figure 3 – Different stages of rotation of the top plate for Topology 1 (a) initial time; (b) half turn; (c) one turn; (d) two turns.

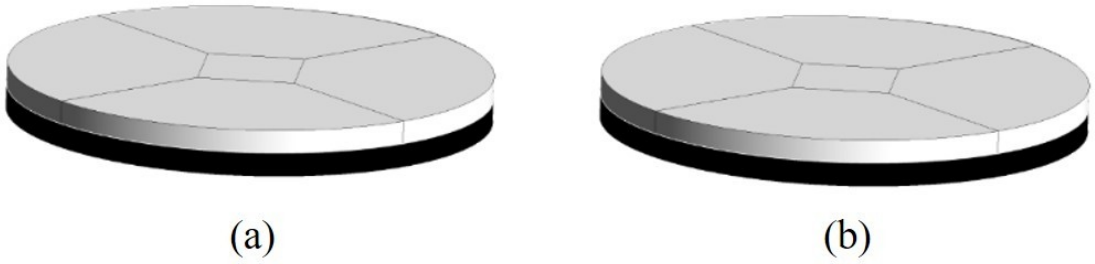

Figure 4 – Two different stages of rotation for Topology 2: (a) initial time; (b) one turn.

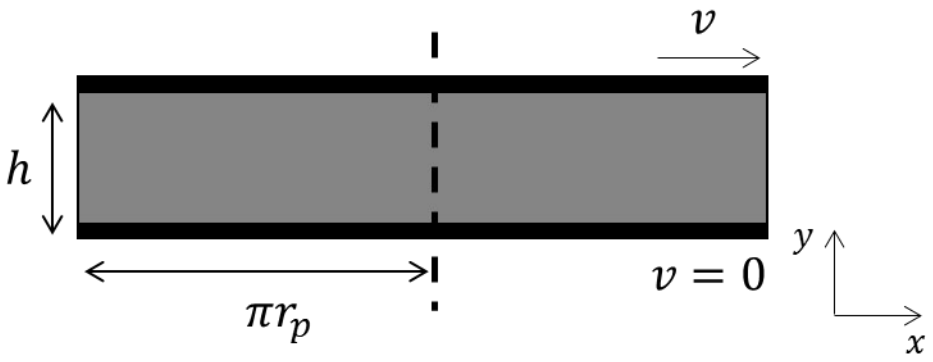

Figure 5 – Sketch of a 2D parallel plates rheometer.

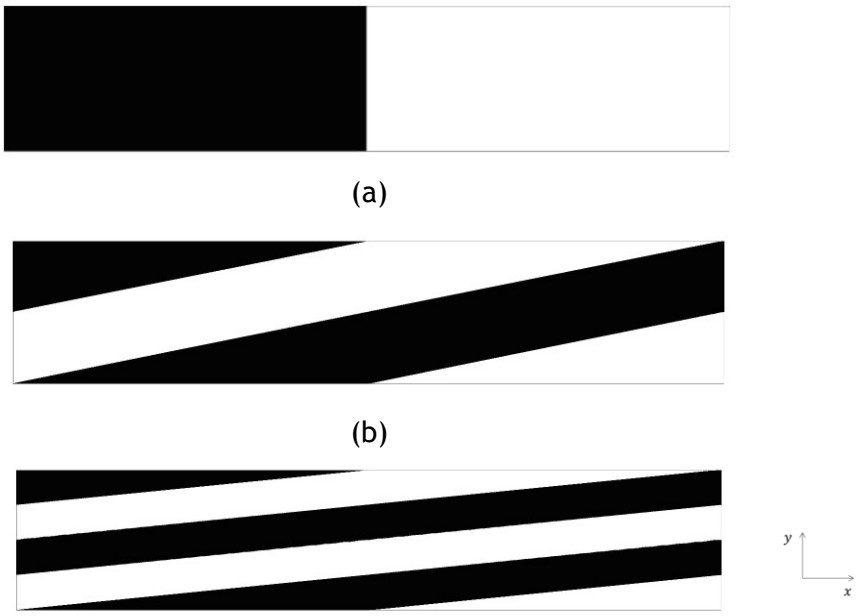

Figure 6 – Contour maps of phases in different stages of rotation for two similar fluids at (a)$N=0$; (b) $N=1$; (c) $N=2$.

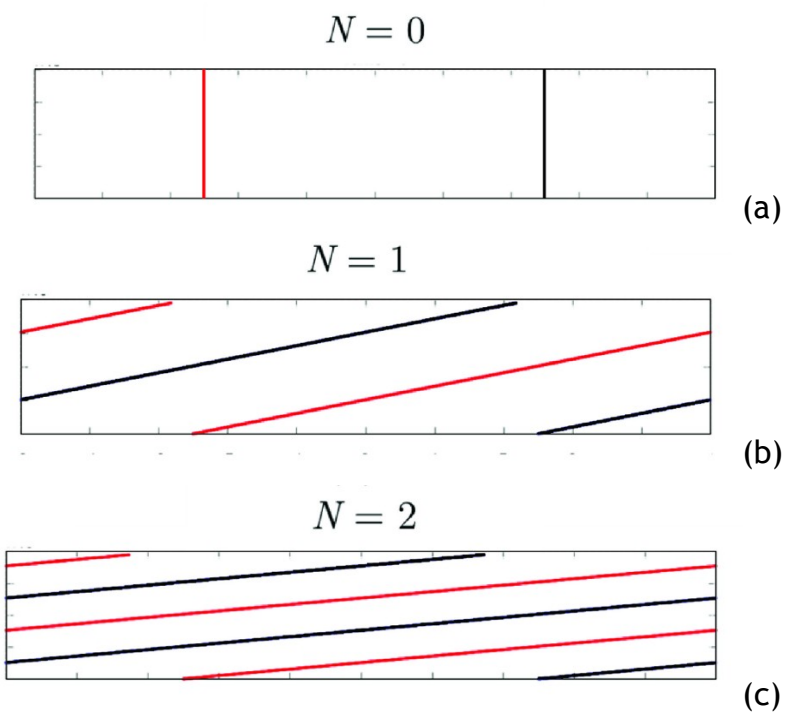

Figure 7 – Position of particles calculated from LMS model at (a) $N=0$; (b) $N=1$; (c) $N=2$.

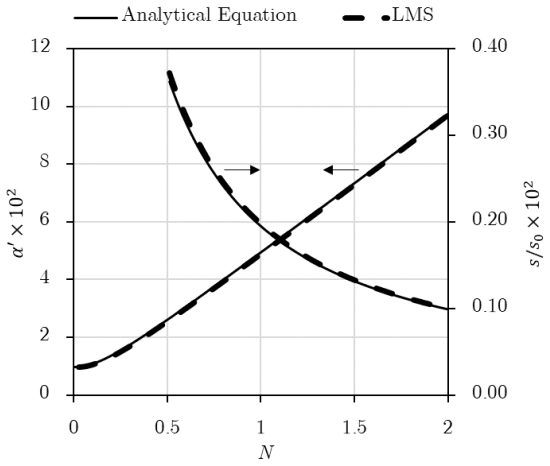

Figure 8 – Interfacial area (α') generation rate and striation thickness (s/s_0) evolution calculated from LMS model for mixing of two similar fluids.

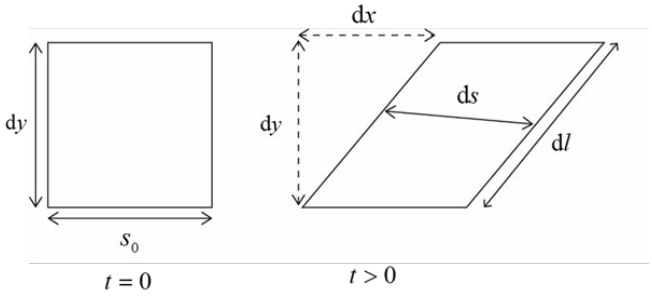

Figure 9 – Stretching of a material element with time in a pure shear flow.

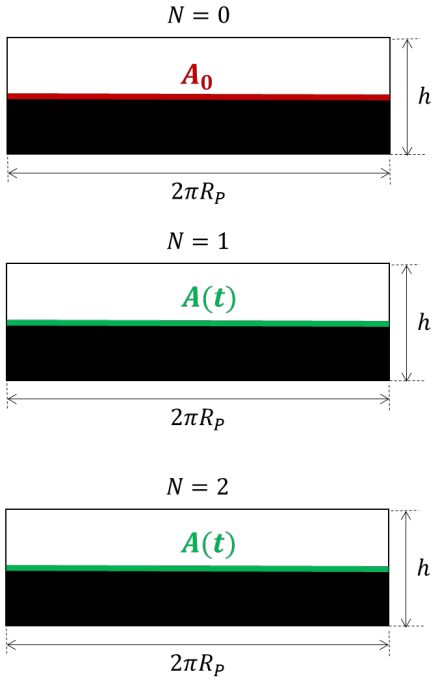

Figure 10 – Sketch of the position of each phase in the outer circle of a 3D plate/plate rheometer for Topology 2 at $N=0$, $N=1$ and $N=2$ where it is tracked the interface between fluids - $A(t)$ for $N=0$ and $A(t)$ for $N=1$ and $N=2$.

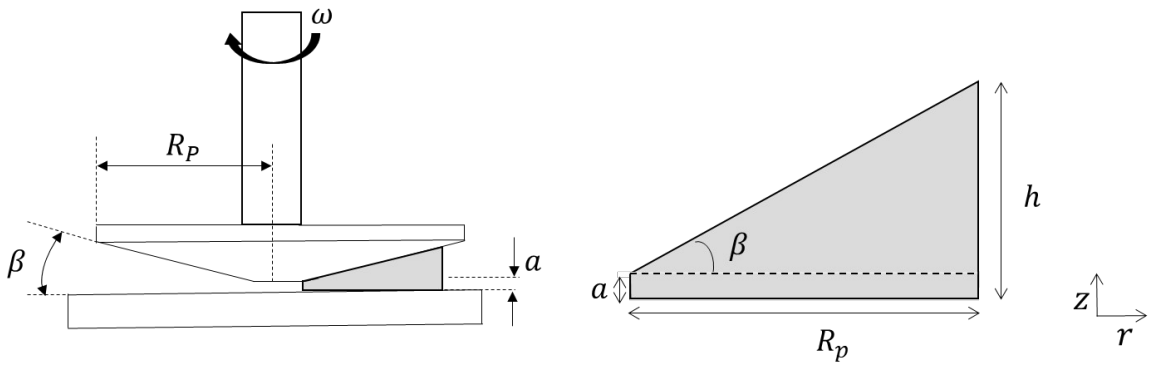

Figure 11 - Schematic representation of the gap between cone and plate and respective dimensions: β is the angle between cone and plate; a is the height of the truncated region; h is the gap between plate and the radius; R_p is the radius of plate.

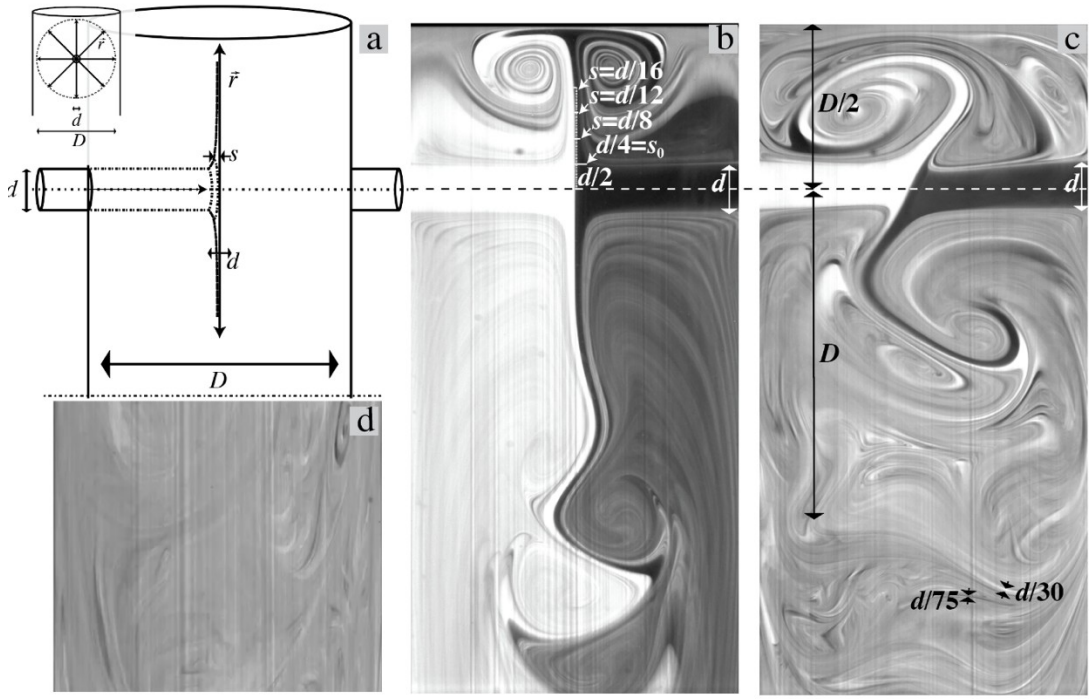

Figure 12 – Analysis of mixing scales in CIJ mixers (a) sketch of CIJ mixers and main flow paths; (b) from PLIF images for segregated flow regime, $\Re = 104$; (c) at the flow regime transition to self-sustainable chaotic flow regime; (d) PLIF image at downstream position >5D from the jets impingement point [32].

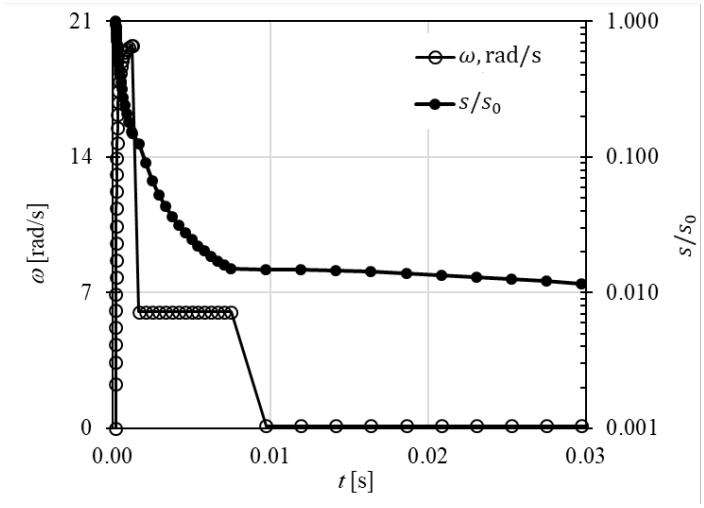

Figure 13 – Shear thinning profile (s/s_0) in a CIJ for a RIM process ($\upsilon_{inj}=4\,m\,s^{-1}$, $d=1.5mm$ and $D=10\,mm$) and a matched profile in a plate-plate device ($r_p=10\,cm$, $h=d/4$) and respective plate angular velocity (ω) [45]

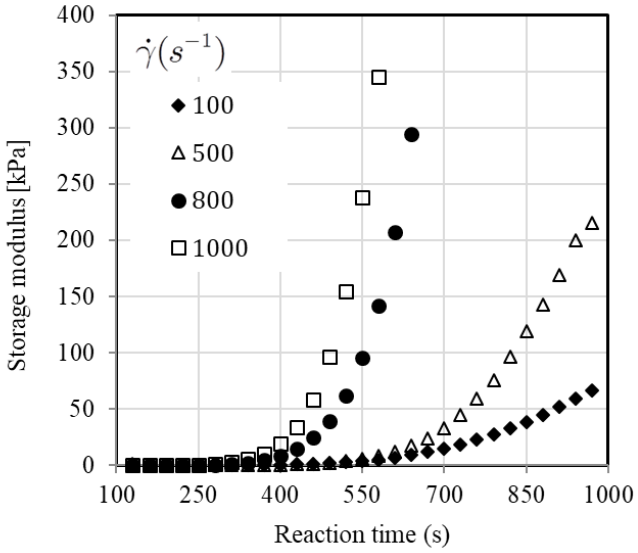

Figure 14 – Storage modulus build-up during a PU curing as a function of pre-mixing shear rate in a cone-plate device ($\beta=0.017\,rad$, $R_P=25\,mm$).